Mixture Design Approach to optimize the rheological properties of the material used in 3D cementitious material printing

Zhixin Liu[1,a], Mingyang Li[1,b], Yiwei Weng [1,c], Teck Neng Wong[1,d*] , Ming Jen Tan[1,e]

[1]Singapore Centre for 3D Printing, School of Mechanical & Aerospace Engineering
Nanyang Technological University, 50 Nanyang Avenue, Singapore 639798

[a]LIUZ0053@e.ntu.edu.sg, [b]LIMINGYANG@ntu.edu.sg, [c]YWWENG@ntu.edu.sg,
[d]MTNWONG@ntu.edu.sg, [e]MMJTAN@ntu.edu.sg

Abstract: The Mixture Design Approach was adopted in this report to formulate the correlation between the cementitious material components and material rheological properties (static yield stress, dynamic yield stress) and identify the optimal material composition to get a balance between high cementitious material static yield stress and low dynamic yield stress. Cement, sand, fly ash, water and silica fume were blended to form the test materials according to mixture design and the responses (static yield stress, dynamic yield stress) were logged by the Viskomat. Two non-linear mathematic models for responses were experimentally validated based on the ANOVA (Analysis of Variance) analysis. The results indicated that the optimal replacement of supplementary cementitious materials can be determined according to static yield stress and dynamic yield stress based on the ternary components. The Mixture Design Approach is then proven to be an effective method of optimizing the cementitious materials used in 3D cementitious material printing (3DCMP) application.

Key words: Additive manufacturing, 3D cementitious material printing, Mixture Design Approach, rheological properties, Multi-objectives optimization, large scale printing

1. Introduction

Additive manufacturing (AM), also known as 3D printing, is gaining more attention from various industries including building and construction due to its advantages: high efficiency, cost effectiveness, labor saving and high freedom of designing [1]. 3D cementitious material printing (3DCMP), which includes Contour Crafting [2], D-Shape [3] and Concrete printing [4], builds the structure without any formwork or mold making, and hence attracts much attention from both the industry and academy sectors in recent years. The fresh rheological properties (static yield stress, dynamic yield stress) of the cementitious material are crucial in 3DCMP field. They can influence the pumpability and buildability of the mixture significantly [5-7]. Cementitious material can only be transported by the delivery system smoothly and then be deposited layer by layer firmly when the pumpability and buildability are appropriate. Hence, various materials have been developed for the 3DCMP by Panda et.al [5, 8-16]. The fresh rheological properties of the developed materials can meet the special requirements of the cementitious material used in 3DCMP. However, few of them investigated the effects of the composites on the fresh properties in a systematic method.

With regard to high flowable material, a huge number of investigations have been conducted to study the effects of the constituents on cementitious material rheological properties [17-26]. Chen et al. [27] reported that the effects of the fine cement on the rheological properties depends on the water cement ratio significantly. According to Jiao [17], the fly ash has a close relationship with rheological properties. The effect of the fly ash on cementitious material fresh rheological properties varies a lot with the change of the shape and the diameter of the material constituents [23, 28]. In most of the cases, material yield stress and plastic viscosity increase with the addition of fly ash content. However,

Park et al. [21] reported that the yield stress of the material without fly ash is higher than that with fly ash content. The lubrication effect, which is important for the pumping of the cementitious material, can be improved by adding silica fume. While most studies show that yield stress and plastic viscosity increase with the addition of silica fume [29-31], Zhang et al [19] showed that silica fume decreases yield stress and plastic viscosity. Ahari et. al [18] reported that silica fume can increase yield stress while reduce plastic viscosity. The reasons for the difference might be twofold: firstly, the surface properties and volume fraction of silica fume in the mixture is various; secondly, the effect of the interaction between the silica fume and content affects the rheological properties [17]. Aggregates affect the rheological properties greatly [10, 26, 32, 33]. Typically, the influence of the composites on rheological properties cementitious material is quite complex. Hence, it is necessary to understand the interaction between the composites when investigating the effects of the composites on the rheological properties in 3DCMP.

Although various experiments have been conducted to investigate the effects of composites on rheological properties, few were conducted in a systematic way in 3DCMP [5, 16, 34, 35]. Hence, a proper model should be constructed through limited experiments. The DoE (Design of Experiments) was adopted to explore individual effects and associate interaction of the cementitious material composites in the mixture on the rheological properties of the cementitious material. It has been successfully used in various fields [36-41]. As one of the most powerful technique of DoE, the Mixture Design Approach was applied in this study. The reasons to select the Mixture Design Approach are threefold: firstly, the sum of the input variables, in this case the volume fraction of individual composites, must be unity. This restricts the range of the component fraction to fit the

model to predict the trend of the rheological properties. Secondly, the rheological properties are assumed to depend on the ingredients fraction rather than the absolute quantity of each component. Thirdly, it can determine the optimal expression of the compound [42].

In this study, the commercial software, Design Expert, was adopted to accomplish the experiments design. The predicted models fit the experimental results with a statistically significance as demonstrated in the ANOVA (Analysis of Variance). The study shows that the Mixture Design Approach is an effective method of understanding the volume fraction of the components on the cementitious material rheological properties used in 3DCMP.

2. Material and methods

2.1 Material formulation

As shown in previous work [43, 44], the cementitious material used in 3DCMP consists of five groups of compounds, Ordinary Portland Cement (OPC, ASTM type I, Grade 42.5), silica fume (SF, undensified, Grade 940, Elkem company), sieved sand, fly ash (FA, Class F) and water. 6g Superplasticizer (SP, MasterPozzolith-R168 from BASF) was adopted to reduce water consumption in each experiment. Fig. 1 illustrates the particle size distribution of cement, SF and FA, which were analyzed by Mastersizer 2000. Fig. 2 presents the particle size distribution of sand, which was analyzed by the sieving machine. Table 1 illustrates the chemical composition of OPC and FA, respectively [43]. The range of the volume fraction of cement is 12%-16%, while the range of the volume fractions of other 4 components were 21%-26%, 25%-30%, 33%-35%, 2%-4% respectively [43, 45].

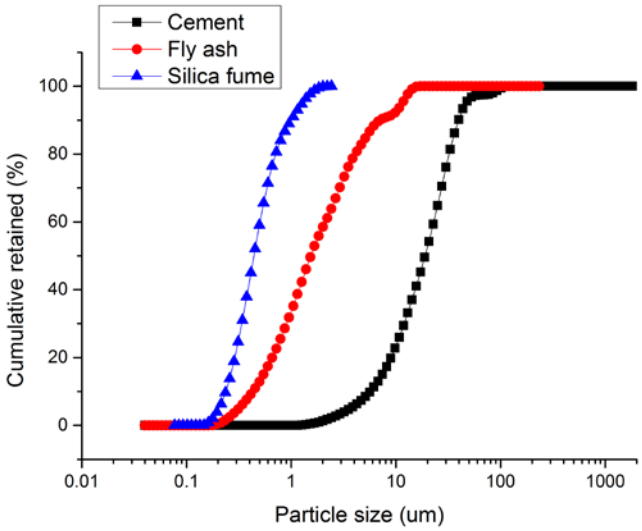

Fig. 1 Particle size distribution of OPC, FA and SF

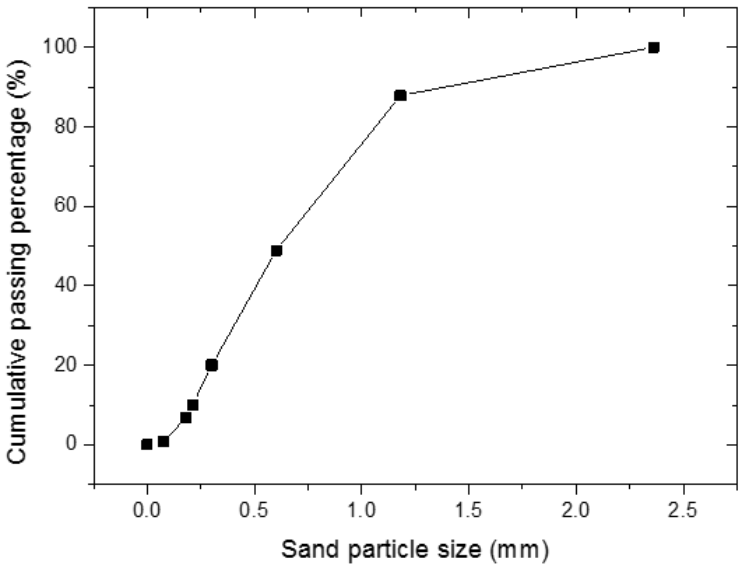

Fig. 2 Sand size distribution

105 Table 1 Chemical composition of fly ash and Ordinary Portland Cement (OPC)

Formula	Concentration / %	
	Fly ash	Cement
SiO2	58.59	24.27
Al2O3	30.44	4.56
Fe2O3	4.66	3.95
TiO2	2.02	0.55
K2O	1.51	0.61
CaO	1.21	62.2
MgO	0.776	3.34
P2O5	0.531	0.15
Na2O	-	0.21
SO3	0.0914	-
ZrO2	0.04	-
MnO	0.0351	-
Cr2O3	0.027	-
CuO	0.0254	-
ZnO	0.0229	-

106

107 **2.2 Mixture design DoE**

108 Due to the variability of the cementitious material properties, it is crucial to design the
109 experiments suited to obtain the feasible compound with various ingredients and accessing
110 their effects on rheological properties. Generally, a series of experiments ought to be conducted
111 by changing the various deliberately one by one. Hence, conclusions can be obtained based on

112 the experimental results. Assume *n* factors exist in an engineering experiment and three
113 control levels for per factor, usually at least 3^n (5 factors and 243 experiments in this study)
114 experiments need to be carefully conducted before the optimal process can be determined
115 based on the traditional experimental process. A scientific approach based on DoE ought
116 to be considered [46], so as to reduce the tedious and costly tests while still allowing
117 insights to be made on overall effects of the variables on the outputs. Only a few
118 experiments that are systematically chosen need to be conducted to separate the individual
119 effects. The theories behind this approach were discussed in [47, 48].

120 In this study, the mixture design DoE was adopted to investigate the effects of input
121 variables (volume fraction of components) on the response (rheological properties). In the
122 mixture design DoE, the response is assumed to depend only on the volume fraction of the
123 components and not on the mass of the ingredients. Mixture designs are constructed based
124 on the upper and lower limit restricted to each component proportion x_i which is defined
125 as a_i (lower limit) and b_i (upper limit)

126 $$0 \le a_i \le b_i \le 1, \qquad \sum_{i=1}^{n} x_i = 1 \tag{1}$$

127 where *i=1,2,3…n.* The response *Y* is a function of the variables x_i.

128 $$Y = f\left(x_1, x_2, \ldots x_n\right) \tag{2}$$

129 The designed experiments in the Mixture Design Approach satisfy the quadratic
130 model

131 $$Y = \sum_{i=1}^{n} \beta_i x_i + \sum_{1 \le i < j}^{n} \beta_{ij} x_i x_j \tag{3}$$

where β_i and β_{ij} are constants, which can be determined by data fitting [49]. n is the number of the compositions.

Typically, the mix design DoE process is listed as follows [42]:

1. Depending on the bound restriction ranges of the variables, pick a suitable mixture design DoE;
2. Determine the name, unit and restrictions of mixture ingredients and the response(s).
3. Propose an appropriate model to correlate the response and the mixture components.
4. Conduct the experiments in order as suggested by the run orders in the model.
5. Input the response values from the experimental results and analyze the responses and variables.

As a powerful statistic method, the testing points were determined in accord with the extreme vertices design method [50], They include the vertices, centers of the plane, bodies and edges of the polyhedron. The determination of the vertices with lower and upper limits were as follows:

a) the maximum range of the variables was calculated by

$$R = 1 - \sum_{i=1}^{n} a_i$$

b) the upper limit of the quasi component was calculated by

$$b_i'' = \min\left\{\left(b_i' - a_i\right)/R, 1\right\}$$

c) b_i''=1, (0,0…I,0…0) was set as the vertices

d) when $b_i'' < 1, b_i'' + b_j'' > 1 (i \neq j)$, $\left(0,...,\overset{i}{b_i''},0,...\overset{j}{b_i''},0,...0\right)$ were the vertices.

e) $b_i'' + b_j'' \leq 1, b_i'' + b_j'' + b_k'' > 1, (i \neq j \neq k)$, $\left(0,...,\overset{i}{b_i''},0,...\overset{j}{b_i''},0,...0,1-\overset{i}{b_i''}-\overset{j}{b_i''},0...0\right)$ were the vertices as well

154 The center of the polyhedron was calculated based on the vertices. More details can
155 refer to [49]. Twenty-two experiments were determined as shown in Table 2.

156 Table 2 The designed cementitious material and specific volume fractions

No.	Cement (%) (x_1)	Sand (%) (x_2)	Fly ash (%) (x_3)	Water (%) (x_4)	Silica fume (%) (x_5)
1	0.160	0.210	0.280	0.330	0.020
2	0.120	0.230	0.300	0.330	0.020
3	0.120	0.210	0.300	0.350	0.020
4	0.120	0.240	0.250	0.350	0.040
5	0.120	0.210	0.280	0.350	0.040
6	0.160	0.210	0.260	0.350	0.020
7	0.140	0.226	0.266	0.339	0.029
8	0.160	0.240	0.250	0.330	0.020
9	0.160	0.210	0.250	0.340	0.040
10	0.140	0.210	0.300	0.330	0.020
11	0.120	0.260	0.250	0.350	0.020
12	0.160	0.210	0.260	0.330	0.040
13	0.120	0.260	0.250	0.330	0.040
14	0.160	0.220	0.250	0.330	0.040
15	0.160	0.210	0.250	0.350	0.030
16	0.140	0.260	0.250	0.330	0.020
17	0.120	0.210	0.300	0.330	0.040
18	0.120	0.260	0.270	0.330	0.020

19	0.160	0.220	0.250	0.350	0.020
20	0.150	0.210	0.250	0.350	0.040
21	0.140	0.226	0.266	0.339	0.029
22	0.140	0.226	0.266	0.339	0.029

Twenty-two cementitious materials were determined according to table which was designed by the mixture design DoE algorithm. The center point, mix design No.7 in Table 2, was replicated three times to provide information about reproducibility [18]. The coefficients of model were determined through the least square method [42] and the prediction models were obtained and they can be used to predict the responses for new observation [49].

2.3 Mixing and testing procedure

Material rheology is greatly influenced by mixing time, rotation speed of the probe in the mixture and temperature [51, 52]. Hence, the same mixing process and measurement were applied for all the batches to keep the rheological properties comparable. The sample volume used for each experiment was 3L and a Hobart mixer was applied in this experiment.

The mixing procedure can be summarized as follows:

1. Dry mixing all the powder ingredients at the speed I for 3 minutes;
2. Remixing water with superplasticizer (6g each batch) and adding them into the mixture. Mixing procedure last 1 minutes at speed II, followed by 2 minutes, at both speed III and IV;
3. Mixing the fresh cementitious material for 1 minutes at the speed of III.

176 The Viskomat XL200, which was also used in authors' previous work [43], was
177 applied in experiments to measure the properties (static yield stress, dynamic yield stress)
178 of the material. To avoid the slippage of material at the surface of the outer cylinder,
179 protruding vanes were fitted at the inner surface of the outer cylinder. For a viscoplastic
180 material, the material is held in the space of the vanes blades and the inner vanes is assumed
181 to be a rigid cylinder. Experimental results in references [53-55] support this assumption.
182 Hence, the assumption was applied in this experiment to derive the rheological properties
183 of the cementitious material as well. The testing procedure is as follows: the material was
184 pre-sheared for 3 minutes, during which the rotational speed gradually increasing from 0
185 rpm to 80 rpm (the pre-sheared stage is essential according to Heirman et. al [56, 57]),
186 followed by a ramp decrease from 80 rpm to 10 rpm (8 steps, each step 30 s) and the
187 transition time between two rotational speeds is 10 s. Rotational speed and torque data
188 points of the viskomat are shown in Fig. 3. It presents the typical sample profile after the
189 cementitious material have been fully pre-sheared. The average torque and rotational speed
190 within each rotational speed step can be one data point in the future regression analysis.
191 The fresh rheological properties (dynamic yield stress) of the cementitious material can be
192 calculated based on Eq. (4) [58]

193 $$T = \frac{4\pi h \ln(\frac{R_o}{R_i})}{(\frac{1}{R_i^2} - \frac{1}{R_o^2})}\tau_0 + \frac{2\pi^2 h}{15 \cdot (\frac{1}{R_i^2} - \frac{1}{R_o^2})} k \cdot N \quad (4)$$

194 The static yield stress can be computed by

195 $$\tau_s = \frac{T_{\max}}{2\pi R_i^2 h} \quad (5)$$

For example, the maximum torque is shown in Fig. 4 for Material No.12 (marked out by the circle). Where T is torque measured at inner cylinder (N·m), N is rotational speed of outer cylinder (rpm), h is the height of the fluid in the viscometer, R_i and R_0 are the radii of inner and outer cylinder respectively.

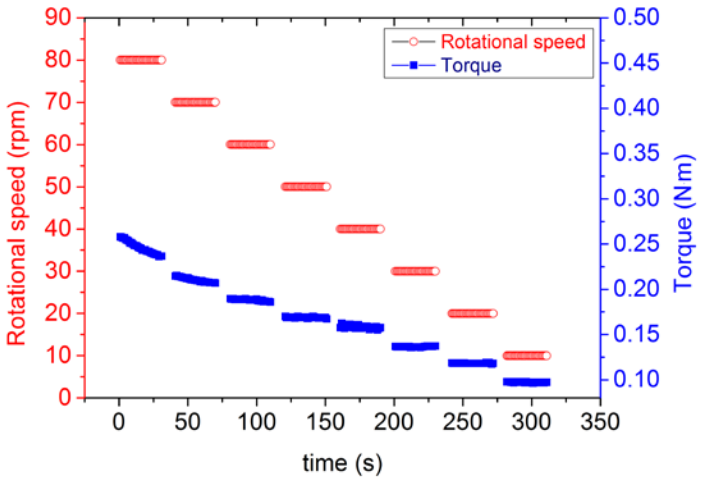

Fig. 3 Rotational velocity and torque data points of rheological tests

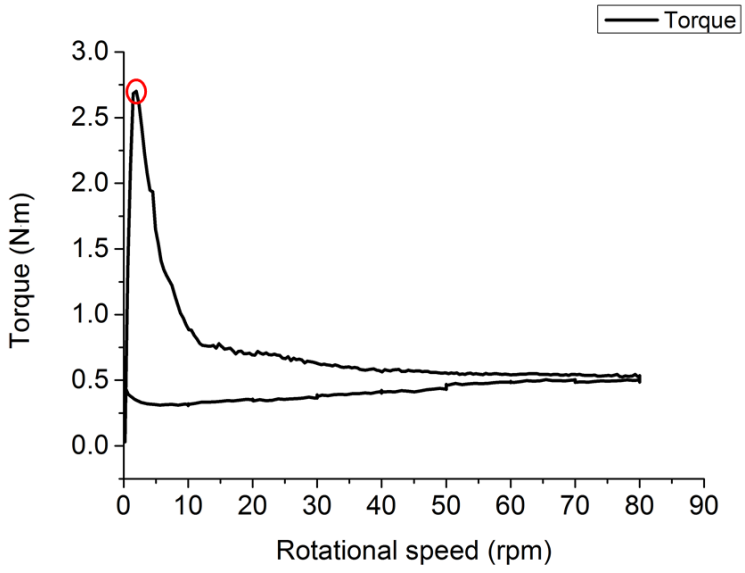

Fig. 4 Torque vs rotational speed for Material No.12

3. Results and discussion

3.1 Measurement of the cementitious material fresh rheological properties

206 The derived rheological properties are listed in Table 3.

207 Table 3 The fresh rheological properties of the cementitious material

No.	Material	Static yield stress τ_s (Pa)	Dynamic yield stress τ_0 (Pa)
1	M1	2363.13	244.81
2	M2	913.88	153.16
3	M3	517.19	70.53
4	M4	576.91	124.41
5	M5	962.93	149.90
6	M6	672.88	98.26
7	M7	1237.27	211.00
8	M8	1346.46	187.22
9	M9	3057.11	322.23
10	M10	572.11	256.26
11	M11	969.86	126.55
12	M12	5952.11	248.16
13	M13	1687.37	208.80
14	M14	5392.64	274.12
15	M15	965.60	154.09
16	M16	540.65	94.07
17	M17	3373.43	271.33
18	M18	497.46	72.67
19	M19	526.25	95.19
20	M20	1775.26	226.39

21	M21	1082.26	168.61
22	M22	1117.42	179.49

Generally, higher water content produces lower static yield stress and dynamic yield stress [17], which is also shown in our experimental results (see Fig. 5, M3, M4, M5, M6, M11, M15, M19, M20). Higher silica fume content generates higher static yield stress, dynamic yield stress as water is absorbed by the silica fume [19]. Among the experimental results, material 12 (M12) and 14 (M14) yield notably higher static yield stress as compared with other materials. The higher static yield stress trend can be attributable to their high silica fume content, which is 4% in volume. However, M4, M5, M9, M13, M17 and M 20 do not produce the high static yield stress even with 4% in volume silica fume. Similarly, M9, M14 and M17 generate higher dynamic yield stress as compared to other materials. For these materials, the higher dynamic yield stress tendency may due to the high silica fume content as well, in this case, 4% in volume fraction. M4, M5, M12, M13 and M20 do not generate high dynamic yield stress even with high volume silica fume yet. It may contribute to the fact that if water or silica fume is the only variable in the experiments, the higher water content produces lower static yield stress and dynamic yield stress, while higher silica fume generates higher static yield stress and dynamic yield stress as the water is absorbed by the silica fume. However, for the experiments in this paper, the total volume of the material is a constant and the individual composite was replaced by each other, which means the volume fraction of each composite changes dependently. At this condition, there is no clear correlation between static yield stress, dynamic yield stress and individual components. Moreover, cement, sand and fly ash did not exhibit clear suppressive effect on static yield stress and dynamic yield stress. This means that the interaction between the

individual components may play an important role on the cementitious material fresh rheological properties.

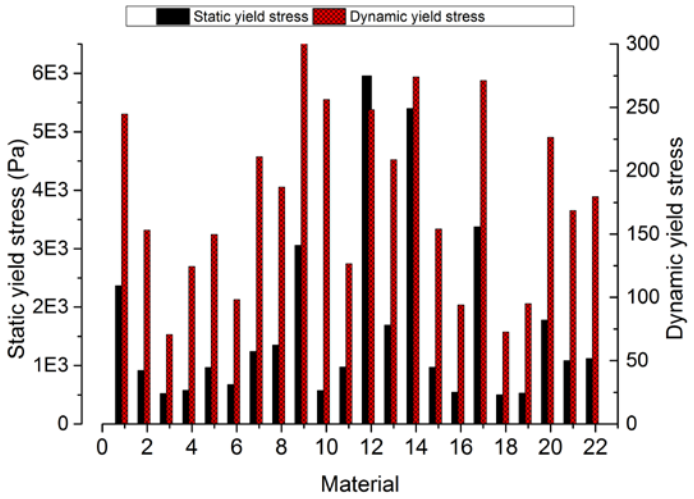

Fig. 5 Rheological properties of various materials

3.2 Analysis of variance (ANOVA) of DoE and fresh rheological models

The quadratic models were adopted to describe the cause and effect correlations between the independent factors (volume fractions of components) and responses (rheological properties) mathematically and statistically. Some insignificant terms were deleted to improve the soundness of the quadratic models. The ultimate results are listed in Table 4. R1, R2 refer to the static yield stress and dynamic yield stress, while x_1, x_2, x_3, x_4, x_5 represent the volume fraction of cement, sand, fly ash, water and silica fume respectively. x_1x_2, x_1x_3, x_1x_5… x_3x_5 refer to the interaction between the individual components.

In ANOVA, P-value and F-value are crucial for evaluating the significance of the DoE proposed model and individual parameters. The P-value is the probability of achieving the F-value. A small P-value implies that the effects of the parameters are statistically significant, while the high F-value indicates the variation reported by the model is

246 significantly larger than that inherent in the process [37]. Table 4 shows the significance
247 of the proposed models with a high F value (72.4 for R1) while very low P-value (<0.0001
248 for R1). This means that there is only a less than 0.01% chance that high F-value of 72.4
249 due to noise. The large P-values (0.079, 0.3736 for R1, R2 respectively) for the lack of fit
250 mean that the model error is not greater than replicate error [38]. Furthermore, high Adeq.
251 precision (>4) indicates that the proposed models incorporating individual components and
252 DoE proposed models for R1, R2 are accurate and statistically significant [36].

253 The ANOVA analysis for the proposed models is shown in Table 4. Some
254 insignificant terms (x_1x_2, x_1x_3, x_1x_5, x_3x_5 for R1; x_2x_5, x_1x_5, x_3x_5 for R2) were removed from
255 the model deliberately to improve the significance of the proposed model. According to
256 Table 4, x_1x_4, x_2x_3, x_2x_4, x_2x_5, x_3x_4, x_4x_5 and x_1x_2, x_1x_3, x_1x_4, x_2x_3, x_2x_4, x_3x_4, x_4x_5, which
257 represent the interactive effects on responses, are regarded as significant terms for static
258 yield stress and dynamic yield stress respectively, except for all the individual components.

259 Table 4 ANOVA table of the mixture design study

Factors	R1		R2	
	F-value	P-value	F-value	P-value
Model	72.35	<0.0001	10.39	0.0004
Linear mixture	128.81	<0.0001	22.76	<0.0001
x_1x_2			5.97	0.0347
x_1x_3			4.35	0.0636
x_1x_4	40.06	<0.0001	9.29	0.0123
x_2x_3	23.45	0.0005	9.09	0.013
x_2x_4	18.68	0.0012	11.95	0.0062

x_2x_5	17.04	0.0017		
x_3x_4	24.23	0.0005	8.26	0.0166
x_4x_5	77.51	<0.0001	10.48	0.0089
Lack of fit	12.17	0.078	2.02	0.3736
R^2	0.985		0.919	
Adj R^2	0.971		0.8311	
Adeq. precision	30.268		11.437	

Fig. 6 shows the normal probability of the internally studentized residuals for R1, R2 respectively in statistics. Studentized residuals is one kind of residuals which can quantify how large the residuals are in standard deviation units. If a testing point has a studentized residual that is larger than 3 (in absolute value), it can be concluded that the testing point is unacceptable. In this work, the points scatter along a straight line, without much deviation. This indicates that the DoE proposed models are accurate even when changing the formation of the models [59].

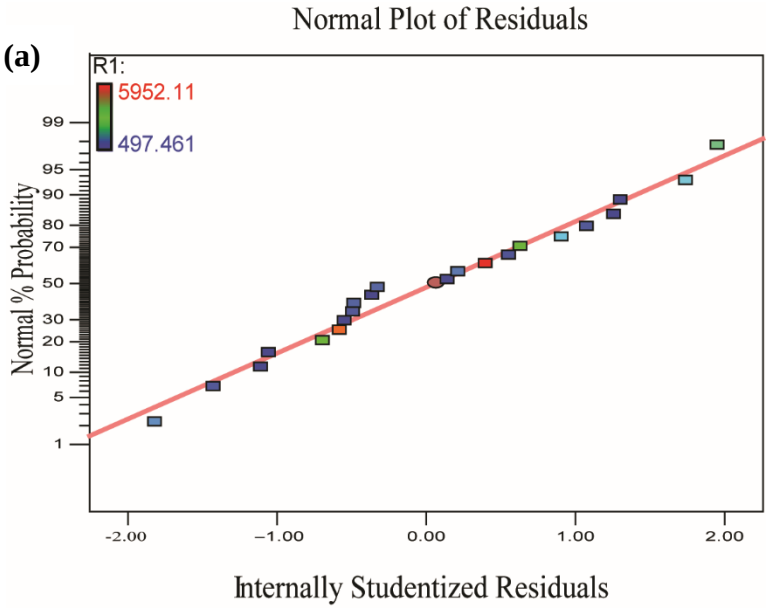

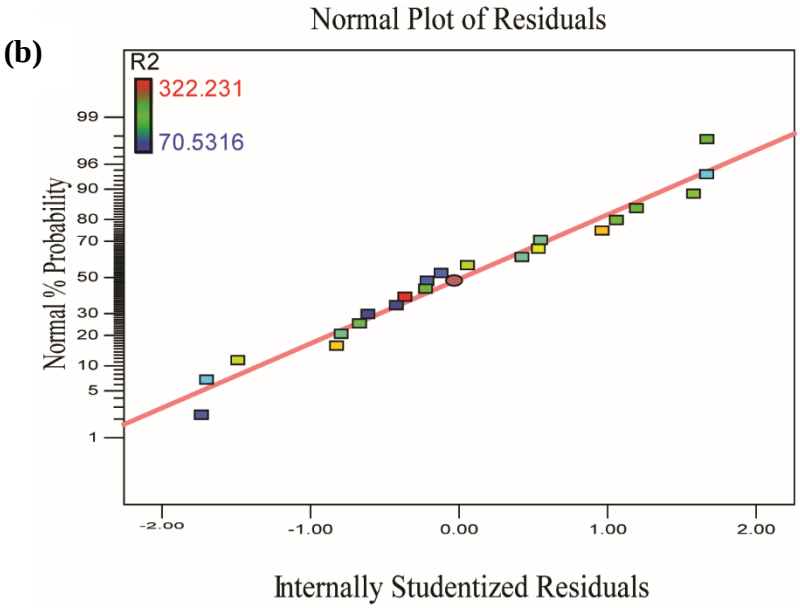

Fig. 6 Normal probability plots of the residuals for (a) static yield stress and (b) dynamic yield stress

To exclude the effects of run order on the presented DoE models, the correlation between the model errors and run order need to be confirmed as well. Fig. 7 shows the residuals versus run orders. No notable trends or groupings were observed and the residuals

scatter randomly around the center line. This indicates that the residuals are independent from one another and this confirms the accuracy of the model [37].

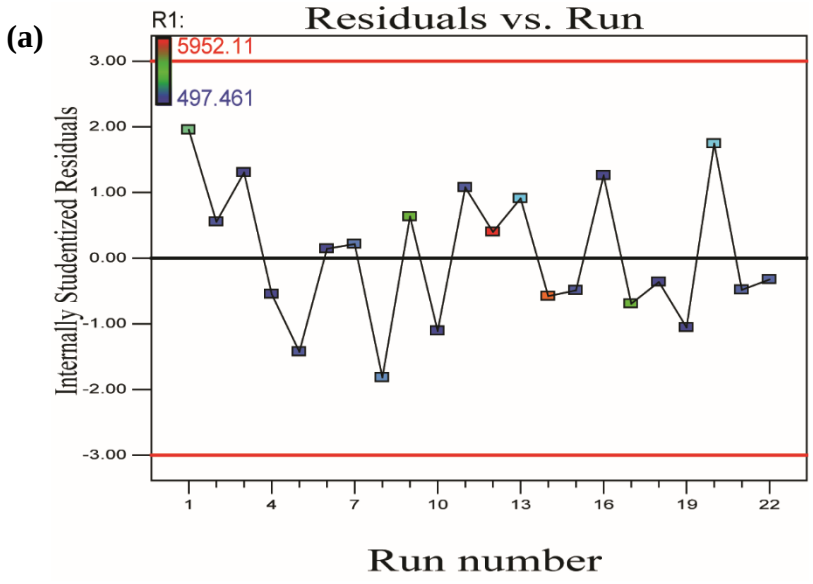

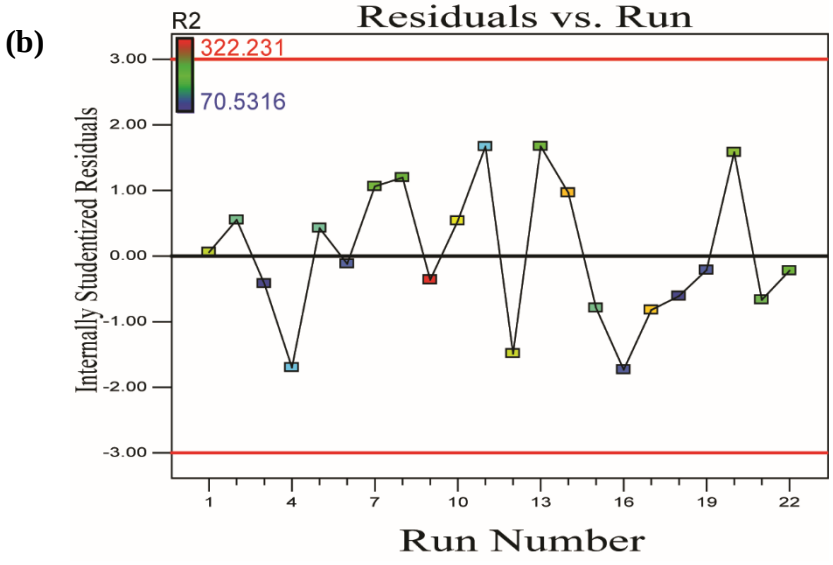

Fig. 7 The relationship between residuals and the run order in which the experiments were performed for (a) static yield stress and (b) dynamic yield stress

Fig. 8 shows the predicted rheological properties (computed from the DoE model) and actual rheological properties (obtained from experiments). The function of the straight line is y(predicted value)=x(actual value). The function can capture the experimental results

well with R^2 are 0.985, 0.919 respectively, which means the relationship between rheological properties and material components were captured successfully by the proposed models.

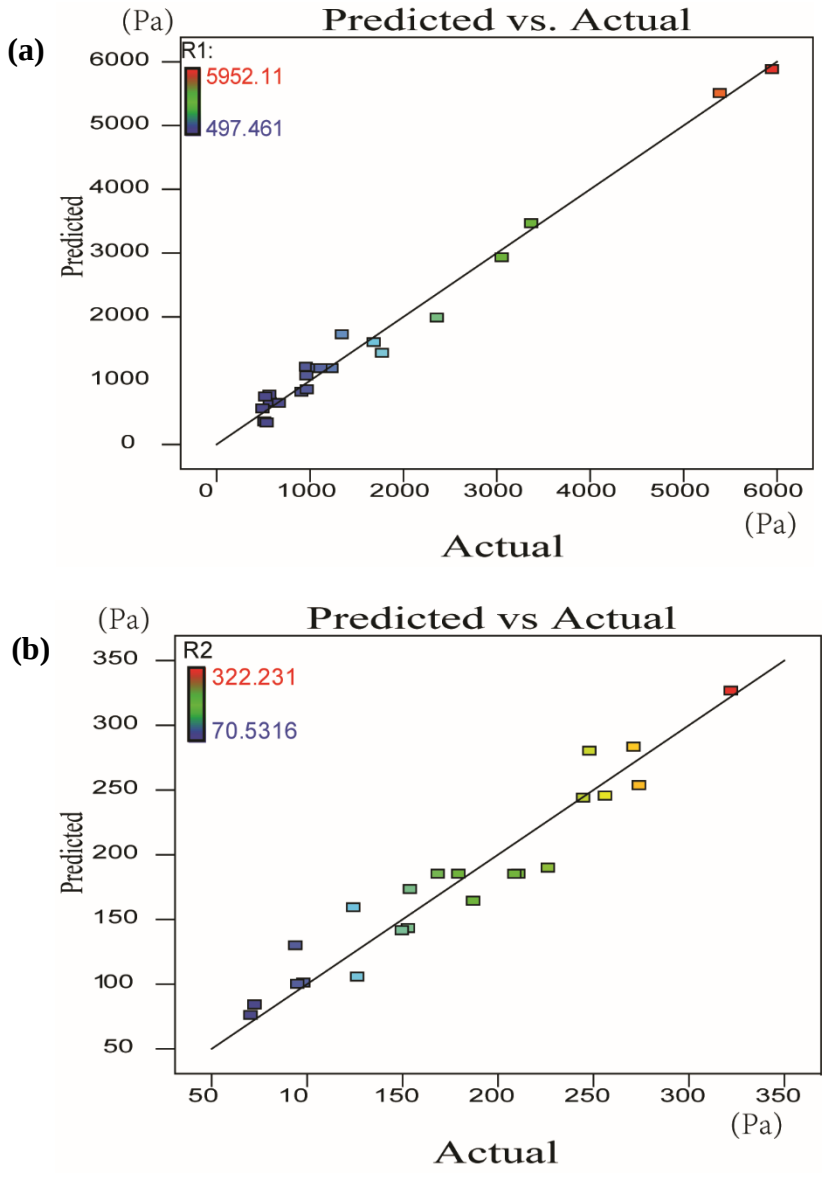

Fig. 8 Predicted rheological properties versus actual rheological properties ((a) static yield stress, (b) dynamic yield stress)

According to ANOVA, the derived rheological models are sound from the statistic perspective. ANOVA confirms the availability of the DoE proposed models, and quantified

causes (volume fraction of each composite) and responses correlations (rheological properties) will be discussed in the next section.

The ultimate models for static yield stress and dynamic yield stress with respect to the five individuals can be expressed as follows:

$$R1 = 10^6(1.78x_1 + 0.19x_2 + 0.54x_3 + 3.59x_4 + 3.83x_5 - 10.28x_1x_4 + 1.42x_2x_3 - 6.68\,x_2x_4 - 1.43\,x_2x_5 - 7.62\,x_3x_4 - 15.3\,x_4x_5) \quad (6)$$

$$R2 = 10^5(-0.32x_1 - 0.64x_2 - 0.28x_3 - 3.23x_4 - 1.62x_5 - 1.16x_1x_2 - 0.99x_1x_3 + 6.72x_1x_4 - 1.43x_2x_3 + 7.65\,x_2x_4 + 6.37\,x_3x_4 + 0.91x_4x_5) \quad (7)$$

4. Optimizing cementitious material components based on rheological properties

Multi-objectives optimization is popular in industry and academic areas [60-62] and will be adopted in 3DCMP area to optimize the rheological properties of the cementitious material as well. Approximate static yield stress and dynamic yield stress are associated with specific cementitious material type and corresponding application. For self-compacting cementitious material, the dynamic yield stress should be low enough to keep material in high flowability. In 3D cementitious material printing area, various factors, such as structuration rate [63], thixotropy [64], stability failure [14, 65, 66] and static yield stress of the cementitious material [43], affect the buildability of the material. According to Perrot et. al [63], while the buildability is proportional to the static yield stress and the geometry factor, the structuration rate of the material affects buildability significantly by increasing the static yield stress when the printing process lasts dozens of minutes. Similarly, the high thixotropy of material can increase the yield stress within short time [64], which then increases the material buildability. When the slenderness ratio is high

enough that the stability failure is dominating, the older stage specimens expand little in lateral direction, however, have a more distinct failure plane with the increase of load in vertical direction due to the relatively high elastic modulus [65, 66]. In the authors' previous work [43], the geometry factor of hollow cylinder has been derived and the buildability for low slenderness ratio structures with short print time was proven to be positive correlated to the static yield stress. Hence, the static yield stress can be used as one of the indicators to characterize the buildability of the fresh cementitious material in 3D cementitious material printing process. However, according to Weng et al.[43], pumpability of the cementitious material is crucial for 3DCMP as well and inversely proportional to the dynamic yield stress. To improve the pumpability of the cementitious material, dynamic yield stress should be as low as possible while remaining good buildability.

4.1 Desirability function approach

Desirability is an objective function, which can reflect the desirable range for each response. It ranges from zero outside the limits to one at the goal. The optimization is to maximize the desirability function. It has been adopted in industry and academic areas to optimize the multi-objectives simultaneously [60, 61]. In this approach, each objective y_i is converted into individual desirability function d_i. If y_i is the most desired value, d_i=1and d_i=0 when objective is outside the acceptable range. In the case of maximization of the response, desirability could be characterized quantitatively based on higher-the-better criteria,

$$d_i = \begin{cases} 0 & y_i < L \\ \left(\dfrac{y_i - L}{T - L}\right)^r & L \le y_i \le T \\ 1 & y_i > T \end{cases} \quad (8)$$

If the response is minimization type, the desirability could be calculated quantitatively based on lower-the-better criteria,

$$d_i = \begin{cases} 0 & y_i > L \\ \left(\dfrac{y_i - L}{T - L}\right)^r & L \le y_i \le T \\ 1 & y_i < T \end{cases} \quad (9)$$

Where r is individual weight parameter related to the objectives and depending on the importance of the objective. L and T refer to the lower limit and upper limit of the response respectively. The lower and higher value assigned to the static yield stress are 497.46 Pa and 5952 Pa respectively and the lower and higher value assigned to the dynamic yield stress are 72.67 Pa and 322.23 Pa.

After calculating the desirability of each objectives, the overall desirability is obtained by combining the individual desirability

$$D = \left(d_1 d_2 ... d_n\right)^{\frac{1}{n}} \quad (10)$$

where *n* is the number of responses in the mixture.

4.2 Effects of components on 3DCMP material rheological properties

The weight parameters are related to the objectives and depending on the importance of the objectives. The greater weight parameter of the objective gives more emphasize to the goal. In this work, static yield stress is much more important during the optimization,

and three different weights parameters were selected for preliminary test. If the weight parameters of static yield stress and dynamic yield stress were 0.8 and 0.2 respectively, the printed filament was discontinuous due to the low pumpability. However, if the weight parameters of them were 0.6 and 0.4 respectively, the buildability tended to be low. Hence, the weight parameters of the static yield stress and dynamic yield stress were set to be 0.7 and 0.3 respectively. In this case, the optimal volume fractions of the five composites (cement, sand, fly ash, water and silica fume) are 0.148, 0.221, 0.261, 0.33 and 0.04 respectively. The desirability is 0.83, which is promising according to Sarteshnizi et al. [67]. At this condition, the static yield stress is 4880 Pa and the dynamic yield stress is 201 Pa. The higher water content produces lower static yield stress and dynamic yield stress while higher silica fume generates higher static yield stress and dynamic yield stress as the water is absorbed by the silica fume. The purpose of the optimization is to generate the high static yield stress, hence the lowest water level and the highest level silica fume were set. Then the effects of the replacement of sand, silica fume and fly ash on the rheological properties were investigated at this condition. When the water content and silica fume content were fixed at 0.33 and 0.04 respectively, the responses (static yield stress and dynamic yield stress) can be plotted on a ternary diagram (an equilateral triangle) with three axes representing the volume fraction of cement, sand and fly ash respectively, as shown in Fig. 9.

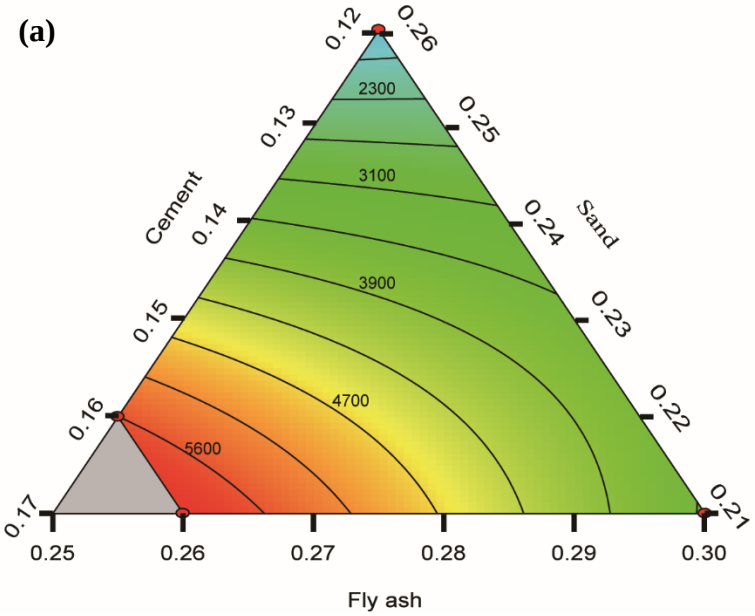

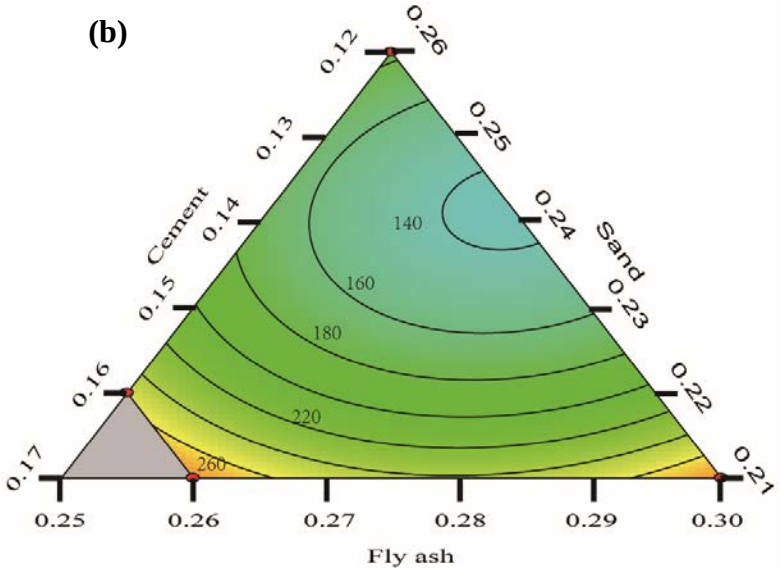

Fig. 9 The contours for (a) static yield stress and (b) dynamic yield stress

The static yield stress and dynamic yields stress contours of cementitious material with cement, sand and fly ash ternary components at given water and silica fume volume fraction were plotted in Fig. 9 (a) and (b), respectively. It is clear from Fig. 9 (a), at the sand volume content higher than 0.235, that the static yield stress contour lines were approximately parallel to the bottom line. This means that for a given high sand volume content, fly ash can be replaced by the same volume of cement with only a slight influence

on static yield stress. In other words, cement and fly ash contribute to the static yield stress similarly when the sand volume fraction is higher than 0.235. The key factors that affects the static yield stress is the friction resistance and interlocking actions. When sand volume fraction is higher, the interlocking and friction resistance are the main factors that contributes to the static yield stress. When the volume fraction of sand is lower than 0.235, material static yield stress increases gradually with the increase of the cement or decrease of fly ash. It seems that cement is more significant than the fly ash in increasing the static yield stress due to the intensive contours at the left bevel. It may due to the fact that with the decrease of the volume fraction of sand, the geometry and rough surface of the cement reduce the particle sliding and increase the friction force, leading to the increase of the static yield stress [68]. From Fig. 9 (a), for example, the static yield stress raises from approximately 4700Pa to 6000Pa with the cement replacement level from 0.15 to 0.16.

From Fig. 9 (b), cementitious material dynamic yield stress decreases with the replacement level of sand less than 0.24 and increases with the rising replacement of fly ash with sand (higher than 0.24). This means that the low volume of sand replacement has a negative effect on dynamic yield stress, while there is an opposite effect when volume of sand replacement is higher than 0.24. This may contribute to the fact that when sand volume fraction is higher than 0.24, with the decrease of the sand volume, the paste volume increases, which can improve the lubrication effect and decrease the dynamic yield stress [68]. The dynamic yield stress increase of the cementitious material may due to the absorption of the unburnt carbon when the sand volume fraction is lower than 0.24.

Apart from that, material dynamic yield stress decreases with the replacement of fly ash up to around 0.28, and then increases with the replacement of fly ash rising. Typically,

when the replacement of fly ash was 0.26-0.27 and the replacement of sand was around 0.24, the lowest dynamic yield stress was obtained from the ternary components contour, where its value is about 140 Pa. In order to aid the visual presentation of the corresponding responses, 3D surface figures were plotted, as shown in Fig. 10. For example, from Fig. 10 (a), the static yield stress rises greatly as the components approach the apex 'x_1', which means that the increase of the cement can lead to a rise of the static yield stress.

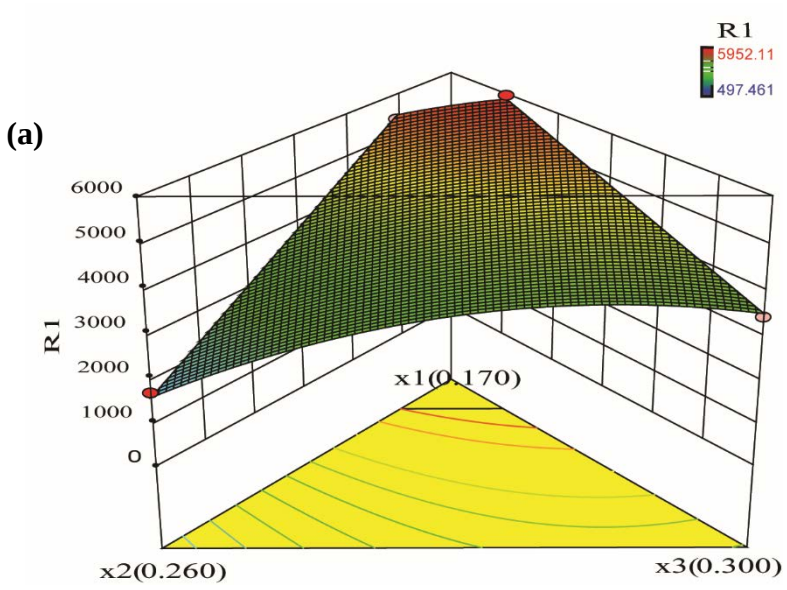

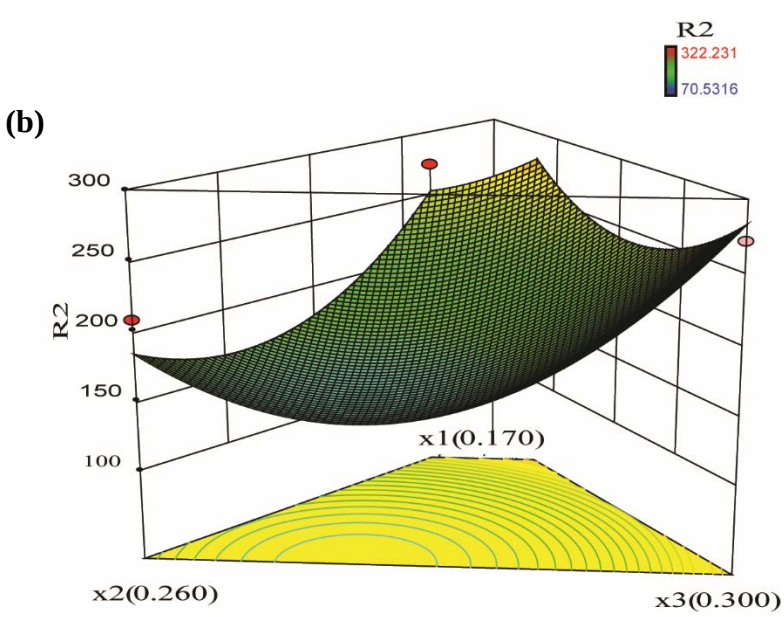

Fig. 10 Response surface diagram in 3D for (a) static yield stress and (b) dynamic yield stress with fixed water volume of 0.33 and silica fume volume of 0.04

4.3 Optimization of composite formulation

From the contours of the static yield stress, when the sand volume fraction is lower than 0.235, the increase of the replacement of the cement or the decrease of the replacement of fly ash can increase the static yield stress. Hence, to make the static yield stress higher than aforementioned optimized static yield stress, the volume fraction of the cement should be higher than 0.148, while volume fraction of the fly ash should be lower than 0.261. From contours of the dynamic yield stress (Fig. 9 (b)), it decreases with the rising of the replacement of fly ash until the replacement reaches 0.28, and decreases with replacement of cement. Hence, to reduce the dynamic yield stress, the range of volume fraction of fly ash should be around 0.28, while the replacement of the cement should be as low as possible. There is a dilemma when increasing the static yield stress and lowering the dynamic yield stress. Hence a compromise needs to be made when trying to capture the low dynamic yield stress and high static yield stress simultaneously.

To ensure the good buildability of the material used in 3DCMP, the static yield stress is set to be higher than 4880Pa. While keeping sufficient pumpability, the dynamic yield stress is set to be lower than 220Pa. According to the analysis of contours, the critical lines of each response can be plotted to meet the requirement, as shown in Fig. 11. The overlap area (Green part) in Fig. 11 is regarded as the optimal components of the cementitious material used in 3DCMP, i.e cement and sand in this study are 0.150-0.155 and 0.215-0.230, respectively.

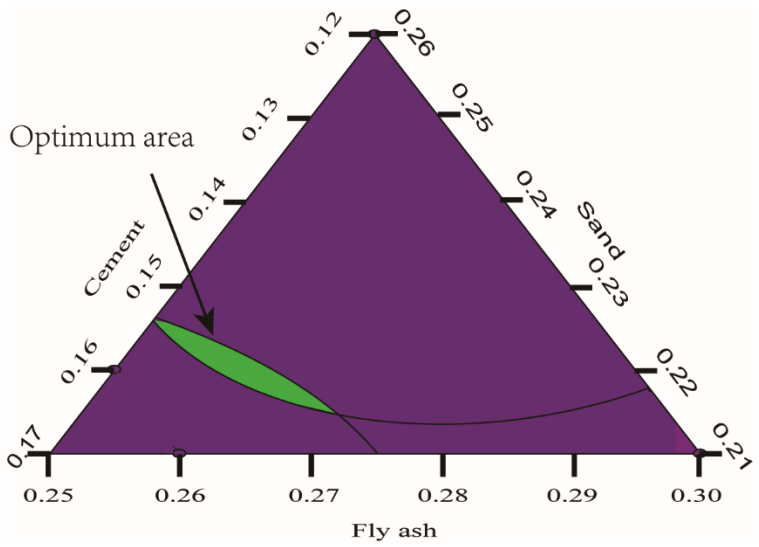

Fig. 11 Optimization mixture for the material used in 3DCMP

5. 3D printing of a large-scale model

According to the discussion above, static yield stress and dynamic yield stress are necessary for 3D cementitious material printing application. The production of a full-size printing is essential to demonstrate the optimized mix design is suitable in practical application.

Fig. 12 and 13 show the components that were printed using a 4-axis gantry concrete printer. They were deliberately designed to show the reliability of using optimized cementitious material for 3DCMP application. The failure printing is shown in Fig. 12. The

445 material selected from zone outside of the optimum area are cement, sand, fly ash, water
446 and silica fume (0.12, 0.25, 0.26, 0.33, 0.04 in volume fraction). Printing failure happened
447 at the 9th layer for this kind of material which indicates that material static yield stress is
448 insufficient to keep the printed layers standing firmly and it is not suitable for 3D
449 cementitious material printing. The successful printing is shown in Fig. 13. It consisted of
450 25 layers with 15 mm thickness for each layer. The length of each printing path is
451 approximately 565.2 mm and nozzle travel speed is 100 mm/s, hence the layer interval time
452 is approximately 5 s. The optimized material, which was randomly selected from the
453 optimum area, used for the large-scale printing material are cement, sand, fly ash, water
454 and silica fume (0.15, 0.22, 0.26, 0.33, 0.04 in volume fraction).

455 Fig. 12 Failure printing with material selected out of the optimum area (only 9 layers)
456

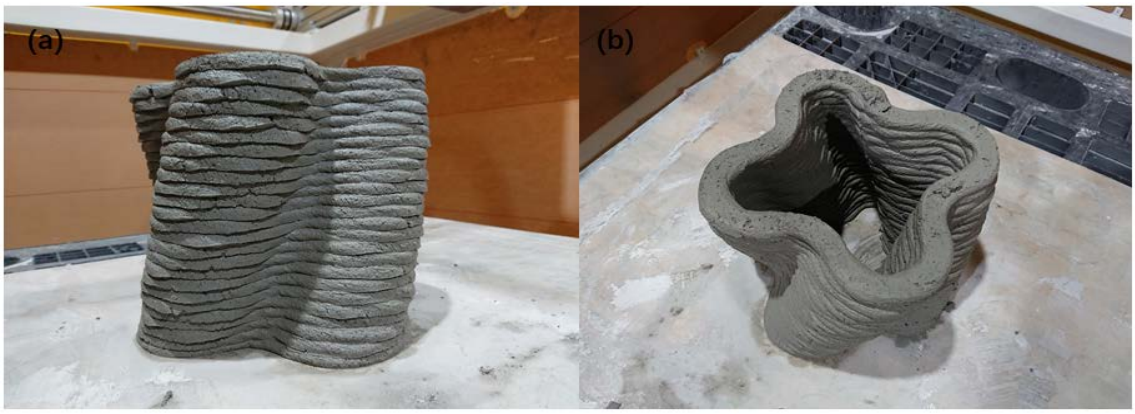

Fig. 13 Successful printing with material selected from optimum area for 25 layers of spiral structure (a) side view, (b) top view

The results show that the Mixture Design Approach is an effective method to optimize the combination of the cementitious material based on fresh rheological properties. In addition, some other cementitious material rheological properties crucial for 3DCMP, such as setting time, open time and plastic viscosity, thixotropy and construction rate can be considered when optimizing the compositions of the cementitious material.

6. Conclusions

In this study, the Mixture Design Approach was proposed to optimize the mixture design of the material used in 3DCMP based on fresh rheological properties. The effects of the ternary system (sand, cement and fly ash) on static yield stress and dynamic yield stress have been evaluated. Based on the specific requirement of 3DCMP, optimization was conducted to determine the acceptable components of the cementitious material. The main conclusions can be summarized as follows:

1. When the volume content of sand higher than 0.235, fly ash can be replaced by the same volume of cement with a slight influence on static yield stress. Material static yield stress increases gradually with an increase of the cement or decrease of fly ash, when the volume fraction of sand is lower than 0.235. However, cement is more

significant than fly ash in increasing the static yield stress due to the intensive contours at the left bevel as shown in Fig. 9 (a).

2. Low volume of sand replacement has a negative effect on dynamic yield stress while there is an opposite effect at high volume of sand replacement (high than 0.24). Apart from that, material dynamic yield stress decreases with the replacement of fly ash up to around 0.28, and then increases with the increase of cement content.
3. When the replacement of cement is 0.26-0.27 and the replacement of sand is around 0.24, the lowest dynamic yield stress is obtained from the ternary components contour, where its value is about 140 Pa.
4. The optimized content of cement and sand in this study are 0.150-0.155 and 0.215-0.230 respectively to make the static yield stress higher than 4880Pa, with the dynamic yield stress kept lower than 220Pa in 3DCMP area.
5. The optimized material adopted for the large-scale printing material were cement, sand, fly ash, water and silica fume (0.15, 0.22, 0.26, 0.33, 0.04 in volume fraction) and large-scale printing showed the reliability of using optimized cementitious material for 3DCMP application.

Acknowledgement

This research is supported by the National Research Foundation, Prime Minister's Office, Singapore under its Medium-Sized Centre funding scheme, Singapore Centre for 3D Printing and Sembcorp Design & Construction Pte Ltd.

References

[1] C.K. Chua, K.F. Leong, 3D Printing and Additive Manufacturing: Principles and Applications (with Companion Media Pack) of Rapid Prototyping Fourth Edition, World Scientific Publishing Company2014.
[2] B. Khoshnevis, D. Hwang, K.-T. Yao, Z. Yeh, Mega-scale fabrication by contour crafting, International Journal of Industrial and Systems Engineering 1(3) (2006) 301-320.
[3] S. Lim, R.A. Buswell, T.T. Le, S.A. Austin, A.G. Gibb, T. Thorpe, Developments in construction-scale additive manufacturing processes, Automation in construction 21 (2012) 262-268.
[4] S. Lim, T. Le, J. Webster, R. Buswell, A. Austin, A. Gibb, T. Thorpe, Fabricating construction components using layered manufacturing technology, Global Innovation in Construction Conference, 2009, pp. 512-520.
[5] S.C. Paul, Y.W.D. Tay, B. Panda, M.J. Tan, Fresh and hardened properties of 3D printable cementitious materials for building and construction, Archives of Civil and Mechanical Engineering 18(1) (2018) 311-319.
[6] G. Ma, L. Wang, A critical review of preparation design and workability measurement of concrete material for largescale 3D printing, Frontiers of Structural and Civil Engineering (2017) 1-19.
[7] Y. Weng, B. Lu, M.J. Tan, S. Qian, Rheology and Printability of Engineered Cementitious Composites-A Literature Review, (2016).
[8] B. Zareiyan, B. Khoshnevis, Interlayer adhesion and strength of structures in Contour Crafting-Effects of aggregate size, extrusion rate, and layer thickness, Automation in Construction 81 (2017) 112-121.
[9] B. Panda, S.C. Paul, L.J. Hui, Y.W.D. Tay, M.J. Tan, Additive manufacturing of geopolymer for sustainable built environment, Journal of Cleaner Production 167 (2017) 281-288.
[10] B. Panda, M.J. Tan, Experimental study on mix proportion and fresh properties of fly ash based geopolymer for 3D concrete printing, Ceramics International 44(9) (2018) 10258-10265.
[11] Z. Li, L. Wang, G. Ma, Method for the Enhancement of Buildability and Bending Resistance of 3D Printable Tailing Mortar, International Journal of Concrete Structures and Materials 12(1) (2018) 37.
[12] M. Xia, J. Sanjayan, Method of formulating geopolymer for 3D printing for construction applications, Materials & Design 110 (2016) 382-390.
[13] T.T. Le, S.A. Austin, S. Lim, R.A. Buswell, A.G. Gibb, T. Thorpe, Mix design and fresh properties for high-

performance printing concrete, Materials and structures 45(8) (2012) 1221-1232.
[14] N. Roussel, Rheological requirements for printable concretes, Cement and Concrete Research (2018).
[15] V. Nerella, M. Krause, M. Näther, V. Mechtcherine, Studying printability of fresh concrete for formwork free Concrete on-site 3D Printing technology (CONPrint3D), Proceeding for the 25th conference on rheology of building materials, 2016.
[16] Y.W.D. Tay, B. Panda, S.C. Paul, N.A. Noor Mohamed, M.J. Tan, K.F. Leong, 3D printing trends in building and construction industry: a review, Virtual and Physical Prototyping 12(3) (2017) 261-276.
[17] D. Jiao, C. Shi, Q. Yuan, X. An, Y. Liu, H. Li, Effect of constituents on rheological properties of fresh concrete-A review, Cement and Concrete Composites 83 (2017) 146-159.
[18] R.S. Ahari, T.K. Erdem, K. Ramyar, Thixotropy and structural breakdown properties of self consolidating concrete containing various supplementary cementitious materials, Cement and Concrete Composites 59 (2015) 26-37.
[19] X. Zhang, J. Han, The effect of ultra-fine admixture on the rheological property of cement paste, Cement and concrete research 30(5) (2000) 827-830.
[20] A.I. Laskar, S. Talukdar, Rheological behavior of high performance concrete with mineral admixtures and their blending, Construction and Building materials 22(12) (2008) 2345-2354.
[21] C. Park, M. Noh, T. Park, Rheological properties of cementitious materials containing mineral admixtures, Cement and concrete research 35(5) (2005) 842-849.
[22] K. Vance, A. Kumar, G. Sant, N. Neithalath, The rheological properties of ternary binders containing Portland cement, limestone, and metakaolin or fly ash, Cement and Concrete Research 52 (2013) 196-207.
[23] C.F. Ferraris, K.H. Obla, R. Hill, The influence of mineral admixtures on the rheology of cement paste and concrete, Cement and concrete research 31(2) (2001) 245-255.
[24] L. Wang, H. Yang, S. Zhou, E. Chen, S. Tang, Hydration, mechanical property and CSH structure of early-strength low-heat cement-based materials, Materials Letters 217 (2018) 151-154.
[25] B. Panda, C. Unluer, M.J. Tan, Investigation of the rheology and strength of geopolymer mixtures for extrusion-based 3D printing, Cement and Concrete Composites (2018).
[26] G. Ma, J. Zhang, L. Wang, Z. Li, J. Sun, Mechanical characterization of 3D-printed anisotropic cementitious material by the electromechanical transducer, Smart Materials and Structures (2018).
[27] J. Chen, A. Kwan, Superfine cement for improving packing density, rheology and strength of cement paste, Cement and Concrete Composites 34(1) (2012) 1-10.
[28] S.H. Lee, H.J. Kim, E. Sakai, M. Daimon, Effect of particle size distribution of fly ash–cement system on the fluidity of cement pastes, Cement and Concrete Research 33(5) (2003) 763-768.
[29] N. Roussel, Rheology of fresh concrete: from measurements to predictions of casting processes, Materials and Structures 40(10) (2007) 1001-1012.
[30] N. Roussel, A thixotropy model for fresh fluid concretes: theory, validation and applications, Cement and Concrete Research 36(10) (2006) 1797-1806.
[31] M. Rahman, M. Baluch, M. Malik, Thixotropic behavior of self compacting concrete with different mineral admixtures, Construction and building materials 50 (2014) 710-717.
[32] J. Hu, K. Wang, Effects of size and uncompacted voids of aggregate on mortar flow ability, Journal of Advanced Concrete Technology 5(1) (2007) 75-85.
[33] M.Y. Yardimci, B. Baradan, M.A. Taşdemir, Effect of fine to coarse aggregate ratio on the rheology and fracture energy of steel fibre reinforced self-compacting concretes, Sadhana 39(6) (2014) 1447-1469.
[34] B. Panda, S.C. Paul, M.J. Tan, Anisotropic mechanical performance of 3D printed fiber reinforced sustainable construction material, Materials Letters 209 (2017) 146-149.
[35] S.C. Paul, G.P. van Zijl, M.J. Tan, I. Gibson, A review of 3D concrete printing systems and materials properties: Current status and future research prospects, Rapid Prototyping Journal (just-accepted) (2018) 00-00.
[36] L. Chen, Y. Ma, Y. Guo, C. Zhang, Z. Liang, X. Zhang, Quantifying the effects of operational parameters on the counting efficiency of a condensation particle counter using response surface Design of Experiments (DoE), Journal of Aerosol Science 106 (2017) 11-23.
[37] L. Chen, Z. Zhang, W. Gong, Z. Liang, Quantifying the effects of fuel compositions on GDI-derived particle emissions using the optimal mixture design of experiments, Fuel 154 (2015) 252-260.
[38] L. Chen, Z. Liu, P. Sun, W. Huo, Formulation of a fuel spray SMD model at atmospheric pressure using

590 Design of Experiments (DoE), Fuel 153 (2015) 355-360.
591 [39] L. Chen, Z. Liang, H. Liu, S. Ding, Y. Li, Sensitivity analysis of fuel types and operational parameters on the
592 particulate matter emissions from an aviation piston engine burning heavy fuels, Fuel 202 (2017) 520-528.
593 [40] Y. Rostamiyan, A. Fereidoon, A.G. Ghalebahman, A.H. Mashhadzadeh, A. Salmankhani, Experimental
594 study and optimization of damping properties of epoxy-based nanocomposite: effect of using nanosilica and
595 high-impact polystyrene by mixture design approach, Materials & Design (1980-2015) 65 (2015) 1236-1244.
596 [41] Y.-f. Tzeng, F.-c. Chen, Multi-objective optimisation of high-speed electrical discharge machining process
597 using a Taguchi fuzzy-based approach, Materials & design 28(4) (2007) 1159-1168.
598 [42] J.A. Cornell, Experiments with mixtures: designs, models, and the analysis of mixture data, John Wiley &
599 Sons2011.
600 [43] Y. Weng, M. Li, M.J. Tan, S. Qian, Design 3D printing cementitious materials via Fuller Thompson theory
601 and Marson-Percy model, Construction and Building Materials 163 (2018) 600-610.
602 [44] Y.W.D. Tay, G.H.A. Ting, Y. Qian, B. Panda, L. He, M.J. Tan, Time gap effect on bond strength of 3D-printed
603 concrete, Virtual and Physical Prototyping (2018) 1-10.
604 [45] S. Mindess, J.F. Young, D. Darwin, Concrete, Prentice-Hall Englewood Cliffs, NJ1981.
605 [46] Y.-H. Lin, Y.-Y. Tyan, T.-P. Chang, C.-Y. Chang, An assessment of optimal mixture for concrete made with
606 recycled concrete aggregates, Cement and concrete research 34(8) (2004) 1373-1380.
607 [47] G. Taguchi, Introduction to quality engineering. 1986, Asian Productivity Organization.
608 [48] A. Garcia-Diaz, D.T. Phillips, Principles of experimental design and analysis, Chapman & Hall1995.
609 [49] Y. Gao, B. Yu, S. Xin, T. Mi, Y. Chen, Q. Yuan, L. Yang, P. Li, Use of Extreme Vertices Method for Analysis of
610 How Proportional Composition Affects Component Interactions and Product Distribution during
611 Hydrothermal Treatment, BioResources 11(2) (2016) 4899-4920.
612 [50] R.D. Snee, D.W. Marquardt, Extreme vertices designs for linear mixture models, Technometrics 16(3)
613 (1974) 399-408.
614 [51] E.-H. Yang, M. Sahmaran, Y. Yang, V.C. Li, Rheological control in production of engineered cementitious
615 composites, Materials Journal 106(4) (2009) 357-366.
616 [52] P. Banfill, D. Swift, The effect of mixing on the rheology of cement-based materials containing high
617 performance superplasticisers, The Nordic Rheology Conference, 2004, pp. 9-20.
618 [53] J.E. Wallevik, Thixotropic investigation on cement paste: Experimental and numerical approach, Journal
619 of non-newtonian fluid mechanics 132(1) (2005) 86-99.
620 [54] M. Keentok, J. Milthorpe, E. O'donovan, On the shearing zone around rotating vanes in plastic liquids:
621 theory and experiment, Journal of non-Newtonian fluid mechanics 17(1) (1985) 23-35.
622 [55] J. Yan, A. James, The yield surface of viscoelastic and plastic fluids in a vane viscometer, Journal of non-
623 Newtonian fluid mechanics 70(3) (1997) 237-253.
624 [56] G. Heirman, L. Vandewalle, D. Van Gemert, O. Wallevik, Integration approach of the Couette inverse
625 problem of powder type self-compacting concrete in a wide-gap concentric cylinder rheometer, Journal of
626 non-Newtonian fluid mechanics 150(2) (2008) 93-103.
627 [57] D. Feys, J.E. Wallevik, A. Yahia, K.H. Khayat, O.H. Wallevik, Extension of the Reiner–Riwlin equation to
628 determine modified Bingham parameters measured in coaxial cylinders rheometers, Materials and structures
629 46(1-2) (2013) 289-311.
630 [58] G. Heirman, L. Vandewalle, D. Van Gemert, O. Wallevik, Integration approach of the Couette inverse
631 problem of powder type self-compacting concrete in a wide-gap concentric cylinder rheometer, Journal of
632 non-Newtonian fluid mechanics 150(2-3) (2008) 93-103.
633 [59] Z. Jeirani, B.M. Jan, B.S. Ali, I.M. Noor, S.C. Hwa, W. Saphanuchart, The optimal mixture design of
634 experiments: Alternative method in optimizing the aqueous phase composition of a microemulsion,
635 Chemometrics and Intelligent Laboratory Systems 112 (2012) 1-7.
636 [60] R.K. Pandey, S.S. Panda, Optimization of bone drilling using Taguchi methodology coupled with fuzzy
637 based desirability function approach, Journal of Intelligent Manufacturing 26(6) (2015) 1121-1129.
638 [61] J. Seo, J.H. Kim, M. Lee, K. You, J. Moon, D.-H. Lee, U. Paik, Multi-objective optimization of tungsten CMP
639 slurry for advanced semiconductor manufacturing using a response surface methodology, Materials & Design
640 117 (2017) 131-138.
641 [62] A. Khaskhoussi, L. Calabrese, H. Bouhamed, A. Kamoun, E. Proverbio, J. Bouaziz, Mixture design approach
642 to optimize the performance of TiO2 modified zirconia/alumina sintered ceramics, Materials & Design 137

643 (2018) 1-8.
644 [63] A. Perrot, D. Rangeard, A. Pierre, Structural built-up of cement-based materials used for 3D-printing
645 extrusion techniques, Materials and Structures 49(4) (2016) 1213-1220.
646 [64] L. Reiter, T. Wangler, N. Roussel, R.J. Flatt, The role of early age structural build-up in digital fabrication
647 with concrete, Cement and Concrete Research (2018).
648 [65] R. Wolfs, F. Bos, T. Salet, Early age mechanical behaviour of 3D printed concrete: Numerical modelling
649 and experimental testing, Cement and Concrete Research 106 (2018) 103-116.
650 [66] A. Suiker, Mechanical performance of wall structures in 3D printing processes: theory, design tools and
651 experiments, International Journal of Mechanical Sciences 137 (2018) 145-170.
652 [67] R.A. Sarteshnizi, H. Hosseini, D. Bondarianzadeh, F.J. Colmenero, Optimization of prebiotic sausage
653 formulation: Effect of using β-glucan and resistant starch by D-optimal mixture design approach, LWT-Food
654 Science and Technology 62(1) (2015) 704-710.
655 [68] D. Jiao, C. Shi, Q. Yuan, X. An, Y. Liu, Mixture design of concrete using simplex centroid design method,
656 Cement and Concrete Composites 89 (2018) 76-88.
657